High power, broadly tunable all-solid-state synchronously-pumped lithium triborate optical parametric oscillator

S. D. Butterworth, S. Girard* and D. C. Hanna

Optoelectronics Research Centre, University of Southampton

Southampton, SO17 1BJ

Tel +44 1703 593147

Fax +44 1703 593142

E-mail sdb@orc.soton.ac.uk

* present address, Laboratoire de Spectroscopie Atomique, CNRS, 6 Boulevard Marechal Juin, 14050 Caen, France.

Abstract:

The performance of a high-power all-solid-state synchronously-pumped optical parametric oscillator (OPO) based on a Brewster-angled lithium triborate (LBO) crystal is reported. The pump scheme includes a diode-pumped amplifier stage to boost the mean output power from an additive-pulse mode-locked Nd:YLF laser by a factor of two. Improvements in the efficiency of an external resonant frequency-doubler have produced a useful output power of 660mW at 523.5nm for pumping the OPO. Temperature-tuned noncritical phase matching of the LBO crystal allowed generation of continuously tunable radiation over the range 0.65-2.7μm with mean output powers for the signal (idler) as high as 210mW (110mW) in the standard X-fold resonator. The high intracavity power of the resonated signal wave introduced nonlinear chirping of the emitted pulses. With prisms to provide intracavity dispersion compensation, nearly transform-limited pulses of 1.63psec duration were generated with mean output power up to 140mW, ie. peak powers of ~700W.

1. Introduction:

The past few years have seen major developments in optical parametric oscillators (OPO's), based on the use of new nonlinear materials, such as lithium triborate (LBO) and capitalising on the availability of improved pump sources having high power and high spatial and spectral coherence. An area of particularly rapid development has been that of synchronously-pumped OPO's, exploiting the wide gain-bandwidth, which allows efficient pumping with short (picosecond or less) pump pulses.

Much of this work on synchronously-pumped OPO's has made use of an Argon laser as the primary pump source, eg. see Powers *et al.* [1] and associated papers in the same special issues. However, the pump power requirements to achieve oscillation threshold are typically low enough to be reached with the peak power produced from a diode-laser-pumped, cw mode-locked Nd^{3+} laser, if additive-pulse mode-locking (APM) is used to produce pulses which are short enough, and hence provide sufficient peak power [2][3]. Preliminary results on performance reported so far for such OPO systems based on LBO have indicated considerable promise for a practical, all-solid-state system [4][5][6].

In this paper we describe in detail the performance of an optimised singly-resonant LBO OPO in which a number of significant improvements have been made over previously reported performance. These improvements include higher pump powers, by making use of a diode-pumped Nd:YLF amplifier stage, and an optimised resonant second harmonic generator, which also uses LBO and gives a 71% external conversion efficiency to the harmonic. Other improvements include a wavelength/cavity length stabilisation scheme (to be described more fully in a separate publication), and the incorporation of prisms for chirp compensation in the OPO resonator. This counteracts the effects of group velocity dispersion

(GVD) and strong self-phase modulation (SPM) as previously reported for femtosecond OPO's in KTP [17][18], but not so far reported for a picosecond OPO. The effects observed in this system are a result of the higher pump powers available and achievement of a very low loss resonator so that a much greater circulating signal intensity results, this being the cause of the significant SPM observed. The result of incorporating the improvements has been the following performance: tuning from 0.65μm to 2.65μm ; mean output powers up to 210mW (110mW) for the signal (idler) respectively. With the incorporation of the prism pair the mean power is reduced to corresponding maximum values of 140mW (72mW) for the signal (idler), the output pulses now being nearly bandwidth- limited and of duration 1.9psec. The combined effect of the chirp compensation and the cavity length stabilisation is to give an output of excellent amplitude and wavelength stability.

A description of the overall system begins in section 2 with a brief review of the characteristics of the self-starting additive-pulse mode-locked Nd:YLF laser, followed by a description of the diode-pumped double-pass amplifier used to increase the output power at 1.047μm from 540mW to 1.05W. Section 3 describes the frequency doubling performance in the external enhancement cavity. Experimental results are compared with an analysis of the cavity which includes the effects of fundamental pump depletion. In section 4, we describe the OPO setup and first present the results of our LBO OPO without GVD compensation. A novel stabilization scheme using a grating optical spectrum analyzer and a position sensitive detector (PSD) to stabilize the cavity length is also briefly described. In section 5, we discuss the results obtained with a combination of intracavity GVD compensation and the active cavity length stabilization. Finally, in section 6, we conclude with some suggestions for future improvements.

2. Nd:YLF APM oscillator and longitudinally diode-pumped Nd:YLF amplifier:

The laser pump source was a self-starting additive-pulse mode-locked Nd:YLF laser pumped by a laser diode. This laser has been previously described in detail elsewhere[9][10]. With a 3W laser diode (SDL-2482-P1), temperature tuned to 792nm, the APM Nd:YLF laser provides 540mW average power. The output consists of Fourier-transform-limited 2.0ps pulses at a 105-MHz repetition rate, corresponding to a 1.4m cavity length.

In order to improve the overall performance of the OPO, it was necessary to increase the available average power from the master oscillator at 1047nm. Scaling up of the oscillator power is limited by the delicate balance of operating parameters needed for the pulse formation process within the APM laser. We therefore preferred to leave the oscillator unchanged and to use an external amplifier. Such a scheme can in principle be scaled up to a considerable extent. Malcolm *et al.*[11] have in fact used two 3-W diodes to pump a Nd:YLF APM oscillator, generating 1W output power, but with some detriment to the pulse duration, which was typically 2.7psec. In our scheme the train of pulses from the main Nd:YLF oscillator were sent on a double-pass through an amplifier rod consisting of a 6-mm long Nd:YLF crystal, longitudinally pumped by a 4W laser diode (SDL-2382-P1). The rod was plane-plane with a 2° wedge to avoid spurious back reflections, AR-coated on the signal-entrance face at 1047nm and coated to be HR at 1047nm and HT at 796nm on the rear (pump-entrance) surface. The output beam from the Nd:YLF oscillator was mode-matched to the gain region with a spotsize of 270μm using an AR-coated lens of 500mm focal length.

The asymmetric beam profile emitted by the diode laser was reshaped to provide a better overlap between the pump and the 1047nm beams, using an arrangement previously reported for an APM Nd:LMA diode-pumped laser[12]. This reshaping of the pump beam also

had a beneficial effect in making the thermally-induced distortion of the crystal, both lensing and distortion of the rear face, more circularly symmetric. The amplified beam was consequently of good circular symmetry, an important factor in the optimization of the second harmonic enhancement cavity (see section 3).

The two-lobed beam emitted by the diode laser was divided by a mirror and then, using a halfwave plate (HWP) and a polarizer beamsplitter cube (PBC), recombined as a single lobe, as shown schematically in figure 1. The main absorption bands in Nd:YLF are centered at 792nm for the π polarization (E$\|$c-axis) and at 796nm for the σ polarization (E$\perp$c-axis)[13]. Adjustment of the laser diode wavelength via temperature control was carried out to maximise the absorption of the pump light, which had roughly equal amounts of the σ and the π polarization. In practice, this optimum wavelength was found to be 796nm, realising a pump power absorption of approximately 70% for the σ and 90% for the π polarization.

For 540mW of average power incident, we obtained 1.05W of amplified output power, corresponding to ~100% gain. The output power versus pump power is presented in figure 2 and shows the absence of saturation as evidenced by the linear slope with no roll-off. As expected the pulse duration was slightly increased from 2.0psec to 2.2psec as a consequence of the power spectrum having been narrowed by the gain profile of the amplifier. However, the pulse duration remains shorter than that reported by Malcolm *et al.*[11] using higher power pumping directly applied to the main oscillator.

Although at this stage, the amplifier is not fully optimized, further improvements of this amplifier using a diode bar as pump[14] should allow multiwatt output power at 1047nm to be attained. With our 105-MHz repetition rate, the output power corresponds to a peak pulse power of 4.2kW. The output beam was then recollimated by a second pass through the

same lens already used to focus the beam into the amplifier.

3. External enhancement cavity for second harmonic generation:

The mode-locked laser was frequency-doubled in a resonant external enhancement cavity, using temperature-tuned noncritically phase matched LBO as the nonlinear crystal. An important step in increasing the pump power available at 523.5nm is to optimize the conversion efficiency of the frequency doubler. The use of resonant external enhancement for SHG was first described by Ashkin *et al.*[15] later extended by Koslovsky *et al.*[16]., and then adapted for mode-locked pump sources by Persaud *et al.*[17].

We have made some modifications to earlier analytical models in order to adapt them for the case where conversion efficiency on a single pass in the nonlinear crystal is large enough that pump depletion needs to be included. Adopting the same notation as in reference 17, the "transmission loss", t_{SH} in the fundamental power resulting from harmonic generation is given by:

$$t_{SH} = \left(1 - \eta_{SH}\right) \tag{1}$$

where η_{SH} is the single pass conversion efficiency. By taking into account the depletion of the fundamental associated with high conversion , the conversion efficiency to the second harmonic for a fundamental circulating power P_C is given by[18]:

$$\eta_{SH} = \tanh^2\left(\sqrt{\gamma_{SH} P_C}\right) \tag{2}$$

The nonlinear conversion coefficient γ'_{SH} for a train of short pulses is derived below and related to the coefficient γ_{SH} for the CW case without pump depletion, defined by:

$$P_{SH} = \gamma_{SH} \cdot P_C^2 \qquad \textbf{(3)}$$

where P_C is the fundamental power circulating through the nonlinear crystal, and P_{SH} is the second harmonic power exiting the crystal. We assume that effects of GVD and SPM within the crystal can be neglected for the case of pulsed harmonic generation so that the second harmonic power as a function of time $P_{SH}(t)$ is again related to the fundamental power by:

$$P_{SH}(t) = \gamma_{SH} P_C^2(t) \qquad \textbf{(4)}$$

Assuming a gaussian temporal pulse shape, and integrating over time, we obtain the following expression for the average powers P.

$$\overline{P}_{SH} = \gamma_{SH} \cdot \sqrt{\frac{2\ln 2}{\pi}} \cdot \frac{1}{\tau_p \cdot f} \cdot \overline{P}_C^2 \qquad \textbf{(5)}$$

where τ_p is the FWHM pulse duration and f (ie. c/2L) the pulse repetition rate. The relation between γ_{SH} and γ'_{SH} is therefore:

$$\gamma'_{SH} = \gamma_{SH} \sqrt{\frac{2\ln 2}{\pi}} \cdot \frac{1}{\tau_p \cdot f} \qquad \textbf{(6)}$$

For an input coupler of power reflectance r_1 , the mean circulating power, P_C of the fundamental can be found by solving numerically the equation:

$$\frac{\overline{P}_{c}}{\overline{P}_{I}} = \frac{(1-r_1)}{\left[1-\left(\sqrt{r_1}\sqrt{T\left[1-\tanh^2\sqrt{\gamma_{SH}\overline{P}_{c}}\right]}\right)\right]^2} \qquad (7)$$

where P_I is the incident average power, T is the combined power transmission of the other three mirrors and other passive losses (except that due to the SH conversion process). The second harmonic average power is obtained by putting P_C in the equation :

$$\overline{P}_{SH} = \eta_{SH}\,\overline{P}_{c}\,\overline{P}_{c}\tanh^2\left[\sqrt{\gamma_{SH}\overline{P}_{c}}\right] \qquad (8)$$

We used a LBO crystal of 12mm length with an aperture 3x3mm^2. The crystal was AR coated at 1047nm and 523.5nm on both faces. The crystal was mounted in an oven and temperature-tuned for Type I noncritical phase matching, with a control of ±0.1°C. The external enhancement cavity was formed by a four-mirror ring resonator. All the mirrors were HR at 1047nm except the input coupler where various reflectivities from 30% to 85% were tested to corroborate our model. The well-known Pound-Drever technique[19] was used to stabilize the cavity length with respect to the Nd:YLF oscillator. One problem encountered was the relatively poor transmission of the $LiNbO_3$ phase modulator we used for the locking scheme, which introduced a loss of 10% and thus only allowed a maximum of 920mW incident average power to be available at the enhancement cavity. The two curved mirrors of 150mm ROC were positioned so as to give a beam waist size for the cavity mode of 27μm at the mid-point between them. The corresponding confocal parameter $b=2\pi w_0^2 n/\lambda$ is equal to 7mm. The nonlinear conversion coefficient γ_{SH} has been calculated by Boyd and Kleinman[20] for a Gaussian beam and is given by:

$$\gamma_{SH} = \frac{2\omega^2 d_{eff}^2 k_\omega}{\pi n^3 \varepsilon_0 c^3} l_c h(B,\xi) \qquad (9)$$

where l_c is the crystal length, n is the refractive index of the crystal at the fundamental wavelength, c is the velocity of light in vacuum, ε_0 is the vacuum permittivity, ω is the fundamental frequency and k_ω the corresponding wavenumber. The effective nonlinear coefficient, d_{eff} , for LBO was determined to be 0.8pm/V by single pass second harmonic conversion measurement with good agreement being obtained for both CW and CW modelocked laser sources.

The focusing parameter $\xi=l_c/b$ was equal to 1.7 and the walk-off parameter B was equal to zero, corresponding to noncritical phase matching (NCPM). According to the numerical analysis of Boyd and Kleinman[20], the value $h(0,\xi)$ is equal to 0.92 for our focussing arrangement.

The CW nonlinear conversion coefficient γ_{SH} was calculated to be $8.9\times10^{-5}W^{-1}$. The corresponding pulsed conversion coefficient γ'_{SH} was $0.25W^{-1}$ for 2.2ps pulses at a 105MHz repetition rate. This high value indicates the need for a model which includes the pump depletion using the $\tanh^2\sqrt{(\gamma'_{SH}.P_C)}$ expression of equation 2 rather than $\gamma'_{SH}.P_C$ which would apply for the undepleted case. In practice, $\gamma'_{SH}.P_C$ gives 0.53 for 2.1Watts incident on the crystal while the $\tanh^2\sqrt{(\gamma'_{SH}.P_C)}$ gives 0.38. ie. a significant correction is involved.

The cavity losses were estimated at 6% per round trip by measuring the power reflected from the input mirror of the resonator when the LBO crystal was detuned from phase matching. The losses are primarily due to the imperfect coatings on the mirrors and crystal, and the scattering in the nonlinear crystal. However, it also contains the losses attributed to the mode-mismatch between the resonated beam defined by the cavity configuration and the

injected pump beam.

We have compared calculated and experimental performance with different reflectivities of the input coupler. Two plots of the theoretical results are shown, one unnormalised, the other normalized to the maximum experimental value. The results, presented in figure 3, give a good agreement between the shape of the experimental and theoretical curves and predicts with a good accuracy the optimum reflectivity. The origin of the discrepancy on absolute value has not been conclusively identified. The best performance was with a 56% reflectivity input coupler at 1047nm. The enhancement of the fundamental power at the crystal compared to the pump power incident on the cavity was calculated to be ~2. The average output power was 660mW at 523.5nm for 920mW fundamental power incident on the input mirror of the cavity, corresponding to an external conversion efficiency of ~72%. For information it should be noted that a single pass through the LBO crystal without the use of an enhancement cavity would give an average power of ~180mW with the same crystal and the presently available pump power. The second harmonic output consists of 2.0ps transform-limited pulses as shown in figure 4, representing a pulse peak power of 2.9kW.

4. OPO without GVD compensation:

The experimental OPO cavity had a linear, rather than a ring configuration, as shown schematically in figure 5. A ring cavity has the benefit of reduced loss and reduced contributions to GVD and SPM due to only one pass through the nonlinear crystal. However, the linear cavity has simpler alignment requirements and was favoured in our experiments for this reason. All the mirrors, curved (100mm ROC) and plane were standard sets from a commercial Ti:sapphire laser (Spectra Physics 3900), the three sets being coated to be highly

reflecting (R>99.9%) over the spectral ranges 650-750nm, 700-850nm and 800-1000nm, and highly transmitting (T>96%) at 523.5nm. The low reflectivity of the mirrors for wavelengths in the idler range (1047nm-2650nm) ensured that only singly resonant oscillation could occur. Mirror reflectivity data were obtained from our own measurements.

At wavelengths longer than 2.4μm there was significant absorption in the mirror coating/substrate which limited the idler output above this wavelength. When output coupling for the resonated (signal) wave was required, one plane mirror was used as an output coupler with transmission of ~3% at the signal wavelength. Similar spectral ranges to those of the HR mirrors were available for this output coupler. The plane high reflector was mounted on a piezo-electric transducer (PZT) for fine cavity length control and the output coupler on a precision translation stage for coarse adjustments.

The Brewster angled crystal was 3x5x15mm^3, cut for type I NCPM in the x-direction (e→o+o) with $\theta=90°$ and $\phi=0°$. This was mounted in an oven designed to vary the temperature between ambient and 220°C with a stability of ±0.1°C. The angle of incidence on the curved mirrors was 13° in order to compensate for the astigmatism introduced into the resonator by the Brewster angled LBO crystal. The calculated waist sizes of the resonated signal wave were 26μmx41μm at the centre of the LBO crystal. The most important advantage of the Brewster-cut crystal is to provide a very low insertion loss over a large wavelength range (cf. narrowband AR coatings) for the horizontally polarized (p-polarised) signal wave. However, this is at the expense of a reduced parametric gain due to the elliptical mode profile in the crystal, and a loss of 18% for the pump light (s-polarized) at the crystal's first surface.

Alignment of the OPO using the standard technique of monitoring the parametric fluorescence proved impractical due to the very low levels of single-pass parametric

fluorescence generated and the close tolerances of the cavity length imposed by synchronous pumping. In order to satisfy the length matching and critical alignment of the cavity, we used a residual beam of ~60mW from the fibre portion of the APM Nd:YLF laser oscillator. This alignment beam was roughly mode-matched to ~450μm at the output coupler of the OPO, through which it was injected into the OPO resonator. Using a system of masks to centre the beam on the mirrors, it was possible to align each mirror in turn, finally overlapping the return beam at the output coupler. Fabry-Perot resonances could then be observed when the cavity is properly aligned and brought into length synchronism. This approach allowed the cavity lengths to be matched to better than 10μm. Three small apertures were then inserted into the cavity and centred on the alignment beam, two between the curved mirrors, on either side of the crystal, with a third in the linear arm close to the output coupler. This defines the optical axis for the signal wave. The pump beam was injected into the OPO, and its transmission through the three apertures was maximised. On removing the apertures and making slight adjustments of the cavity length, oscillation would occur when the length adjustment achieved synchronism of the signal and pump pulses. This procedure gives a simple technique for alignment. Small iterative adjustments to the focusing optics and cavity alignment then provided the maximum output. The OPO threshold in this configuration was measured to be 170mW of average power incident on the input mirror to the cavity for an output coupler transmission of 2.5%. This threshold value, and other values obtained for different output coupler transmissions were found to agree with our calculated values to within ~10%. An earlier estimate of LBO thresholds, made by McCarthy and Hanna[21] was significantly lower as a result of using an assumed d_{eff} of 1.2pm/V (now revised to 0.8pm/V), and due to omission of the numerical factor analogous to the focussing parameter $h(B,\xi)$ in

equation 9, which should be included for the case of noncritical phasematching. Guha *et al.*[22] have analyzed the case of optimum focussing for a singly resonant oscillator and derive values for the appropriate focussing parameter. Interpolation of their published data for the conditions appropriate to our OPO gives excellent agreement between predicted and observed threshold.

Interestingly, the best output power performance was obtained with the LBO crystal offset so that its centre was ~5mm away from the pump waist, corresponding to a situation where the highest pump intensity, ie. pump waist, with undepleted pump, is presented at the input face of the crystal. The maximum output power obtained for the signal was >200mW, at 720nm, but the overall conversion efficiency (signal+idler) remains roughly constant over the major part of the tuning range, as shown in figures 6(a,b). The corresponding conversion efficiency internal to the crystal, deduced from pump depletion measurements, was ~75%. The OPO was tuned by varying the temperature of the crystal oven over the range 176°C-120°C. The combined tuning range for signal and idler was extended from our earlier reported results [5] by the use of the third set of mirrors (650-750nm) and is shown in figure 7. A small region close to degeneracy from 1000nm to 1100nm suffered from idler feedback, so that although the threshold was very low (<10mW), it led to the characteristically unstable performance associated with a doubly resonant oscillator (DRO). Over the rest of the tuning range, stable singly resonant oscillation occurred. The solid and dotted curves represent the calculated tuning range using the temperature-dependent Sellmeier equations for LBO given by Lin *et al.* [23] and Kato[24] respectively.

Measurements of the OPO output pulse duration were made by both second order intensity and interferometric autocorrelation techniques. The spectrum was recorded simultaneously using an optical spectrum analyzer having a resolution of 0.1nm. The intensity

autocorrelation measurement provides the duration of the OPO pulses while the interferometric autocorrelation and the spectrum provide information on the optical frequency chirp induced in the optical pulse by group velocity dispersion (GVD) and self-phase modulation (SPM). Pulses with a frequency chirp give rise to a spectral broadening and an interferometric autocorrelation trace with destructive interference in the wings[25]. Results from the OPO without any dispersion compensation are shown in figures 8 (a,b,c).

Measurements have been performed with different circulating powers by inserting an iris into the OPO cavity to introduce loss and so reduce the level of oscillation without modifying the pump power. Measured pulse durations were found to increase from 1.4ps to 2.3ps as the circulating power was increased from 0.76W to 5.4W. The corresponding spectral broadening was from 600GHz to 1.4THz with significant modulation at higher powers indicative of self-phase modulation. It should be noted that the NCPM bandwidth is calculated to be 796GHz at degeneracy. The time-bandwidth product at maximum output power was 3.3, which is ~10 times the Fourier transform limit for $sech^2$ pulses. The loss of fringe visibility (fig 8(c)) in the wings of the interferometric autocorrelation at high power provides further evidence of the non bandwidth-limited nature of the pulses.

The chirping depends strongly on the circulating power, indicating that besides a linear contribution to chirp from GVD a role is also played by nonlinear effects such as SPM or cascaded second-order effects[26]. Similar effects have already been reported in a Ti:sapphire pumped KTP:OPO by different groups [27],[28]. J.M. Dudley *et al.*[8] presented a simple calculation to estimate the consequences of SPM for a pulsed OPO, in terms of both pulse and spectral broadening. The value of n_2 for lithium triborate has recently been determined using the z-scan technique and is found to be $3.4(\pm 0.8)\times10^{-16}$ cm^2/W [29]. The following

$$\phi_{SPM} = \frac{2\pi . n_2 . l_c . I_p}{\lambda_s} . 2 . N \qquad \textbf{(10)}$$

parameters have been used in conjunction with equation (10) to obtain an estimate of the nonlinear phase-shift. l_c is the crystal length of 15mm, λ_S is the signal wavelength of 855nm, I_P is the on-axis peak intensity of 2.68×10^{13} W/m^2 for an intra-cavity power of 8 Watts, N is the number of round trips experienced by the signal photons. This is equal to 1/(round trip loss), ie. $\sim 1/T_{OC}$ where T_{OC} is the transmission of the output at λ_S (2.5%), this being the dominant loss. The factor of 2.N is used since in this standing wave OPO cavity, although gain is only seen on one pass through the crystal per round trip, the nonlinear phase shift is present on both passes of the crystal. Using these parameters we obtain a nonlinear phase-shift ϕ_{SPM} of 2.5π, thus confirming that significant SPM effects are to be expected under our operating conditions.

As well as producing phase modulation on the OPO pulses, the high intracavity power is sufficient to generate significant amounts of second harmonic light. For example, with the OPO tuned to a signal wavelength of 850nm, blue light corresponding to the second harmonic of the signal was emitted with a mean power in excess of 1mW. This amount of blue light was found to agree with the value calculated for the corresponding phase-mismatch obtained from the Sellmeier equations ie. the power generated within several coherence lengths. The blue light power decreases as the OPO is tuned away from degeneracy, as expected, because the higher dispersion at shorter wavelengths increases the phase mismatch.

The susceptibility of the OPO to cavity length detuning was measured by ramping the PZT at 10Hz and monitoring the output power (this is shown in figure 10). The OPO was

found to tolerate a total cavity length detuning of ~30μm. The output power variation is asymmetric with length detuning, dropping very quickly when the cavity is detuned to longer lengths and more slowly for shorter lengths. The length detuning results in a shift of oscillation wavelength, tuning over a range of as much as 15nm around 800nm and nearly 50nm at 950nm. This monotonic shift of the oscillation wavelength with cavity length has been used to provide a means of stabilising the wavelength via feedback control of the cavity length, thus suppressing the wavelength fluctuations arising from mechanical vibrations or environmental perturbations in the optical path (thermal expansion of the optical bench and optical components, air-index variations etc.). Without any stabilization, the emitted wavelength of the OPO could fluctuate randomly around its central value by ~3nm typically.

The scheme used to actively control the length of the OPO is based on the method developed by Chesnoy *et al.*[30] for a CPM dye laser and adapted for an OPO by Wachman *et al.*[7]. The setup of our feedback loop stabilization is represented in figure 5. A small part of the OPO beam is reflected off a glass plate and sent at grazing incidence on to a 1200 lines/mm optical grating. The diffracted beam is focused by a cylindrical lens onto a position sensitive detector (PSD) The signal detected by the PSD is compared with a reference level, and the differential signal feeds a high-voltage amplifier, whose output is applied to the piezo-electric transducer on which the rear HR mirror of the OPO cavity is mounted. Using a PSD in place of the two photodiodes used by Chesnoy *et al.*[30], provides both simplicity and high resolution. A more detailed description of the stabilization scheme and the experimental performance will be described elsewhere [31].

5. OPO with GVD compensation:

To compensate the pulse chirping in the OPO, we used a pair of highly dispersive SF10 prisms in the OPO cavity. According to the theoretical calculations developed by Fork *et al.*[32], a double pass though a prism pair gives a second derivative of the phase with respect to frequency:

$$D_{2P} = \frac{d^2\phi_P}{d\omega^2} = \frac{\lambda^3}{2\pi c^2}\cdot\frac{d^2P}{d\lambda^2} \tag{11}$$

where the derivative of the optical path P with respect to the wavelength is [33]:

$$\frac{d^2P}{d\lambda^2} = 4.\left[\frac{d^2n}{d\lambda^2}+\left(2n-\frac{1}{n^3}\right).\left(\frac{dn}{d\lambda}\right)^2\right].d\tan\frac{\alpha}{2} - 8.\left(\frac{dn}{d\lambda}\right)^2.\left(l+d.\tan\frac{\alpha}{2}.\tan\frac{\epsilon}{2}\right) \tag{12}$$

where n is the SF10 index of refraction at wavelength λ, α the prism apex angle, ε the deviation angle, d the prism insertion (ie. the distance from the resonated beam in the prism to the prism apex) and *l* the separation of the prism apices when d=0. At the minimum of deviation, the angle of incidence corresponds almost to the Brewster angle and ε can be calculated knowing the n and α values.

For a given distance *l* and an insertion d, the overall negative GVD introduced can be calculated by using the relations above and the Sellmeier equations for SF10 glass[34]. In a first step, we neglect the phase shift introduced by nonlinear effects such as SPM. The minimum negative GVD must be at least equal to the positive GVD arising from the LBO material dispersion. For a single pass though l_c=15mm LBO crystal, the positive GVD can

be calculated by:

$$D_{2C} = \frac{d^2\phi_C}{d\omega^2} = \frac{\lambda^3 l_C}{2\pi c^2} \cdot \frac{d^2 n}{d\lambda^2} \qquad (13)$$

Using the Sellmeier equations for LBO given by Lin *et al.*[23], we estimated a quadratic phase distortion for the ordinary wave at 800nm of D_{2C}= +723fs^2 per pass in the nonlinear crystal (D_{2C}= +1446fs^2 per round trip). For a fixed prism separation *l*=25cm, the prism insertion to compensate the linear GVD in the LBO crystal was calculated to be d=8mm. In practice, the prism insertion d was adjusted (keeping *l* fixed) to optimise the compensation of the nonlinear chirping.

The alignment technique used to insert the prism pair in the cavity was similar to that described by Dudley *et al.*[8]. With the OPO initially oscillating without prisms, the apex of the first prism was slightly inserted into the optical path of the resonated wave, refracting a small amount of signal light but still maintaining parametric oscillation on the undeviated path. The refracted beam was then used to align the second prism and the rear plane mirror mounted on a PZT. By ramping the position of the rear mirror with the PZT, Fabry-Perot fringes could be observed when the length of the second arm containing the prism pair was adjusted into synchronism. Then, the first prism was inserted further onto the optical path to refract all of the signal beam. The rear mirror was translated forward to compensate the increased amount of glass introduced into the optical path by the first prism. The OPO oscillated when the cavity was again brought into synchronism.

The optimum prism insertion was found to be equal to d=4mm with a prism apex separation *l*=25cm. According to the previous calculations, the corresponding quadratic phase shift was D_{2P} = -2940fs^2 which indicates that the prism pair not only compensates the linear

dispersion of the LBO crystal but also compensates the nonlinear effects such as SPM. The temporal and spectral characteristics of the output signal pulses from the GVD- compensated OPO are presented in figures 11(a,b,c). The pulse duration was reduced to 1.63psec assuming a $sech^2$ fit to the intensity autocorrelation. The corresponding spectral width was 303GHz giving a time-bandwidth product of 0.5, ie ~1.6 times larger than the Fourier-transform limit for a $sech^2$ pulse. The interferometric autocorrelation trace (figure 11c) was essentially chirp-free, and the shape of the minimum and maximum envelopes corresponds to the pulse duration estimated with the intensity autocorrelation. Although the average output power is reduced as a result of the prism losses, a good average power could still be achieved, eg. ~140mW at 800nm.

When using the prism pair, the cavity length stabilization was found to be particularly beneficial, giving much better stability of output power and wavelength. Furthermore, the prism insertion could be slightly adjusted simultaneously with the rear mirror position, thus eliminating any wavelength shift, and maintaining parametric oscillation.

6. Conclusions and future developments:

Through the addition of a simple double-pass diode-pumped Nd:YLF amplifier we have been able to achieve an average power of 1.05 Watts of 1.047μm laser light in the form of 2.2 psec pulses with peak powers of 4.2kW. With a fully optimised resonant frequency doubler we achieved 71% (78%) external (internal) harmonic conversion efficiency, producing 660mW of useable output power at 523.5nm.

We have reported the operational characteristics of a widely-tunable synchronously-pumped singly resonant OPO based on a Brewster-angled lithium triborate crystal. The full

tuning range of 0.65-2.65μm with this device has been realised through the use of three mirror sets. Output powers of greater than 200mW (90mW) have been demonstrated for the signal (idler) respectively. The much increased intra-cavity circulating powers introduce significant chirping effects, not previously reported for a parametric oscillator in the picosecond regime through a combination of group velocity dispersion (GVD) and self-phase modulation (SPM) effects. These effects have been compensated by a pair of intracavity SF10 prisms. This results in the generation of nearly transform-limited pulses with duration of 1.6psec.

Reliable, stable long-term operation, both in wavelength and output power has been demonstrated through the addition of an active cavity-length stabilisation scheme, which has proved particularly useful when operating the OPO with GVD and SPM compensation.

While the aim of this work, to demonstrate a reliable all-solid state widely tunable OPO, has been achieved, there remain a number of improvements that can be made, particularly in reducing the complexity of the pump source for the OPO. The demonstration of Kerr-lens modelocking (KLM) of a Nd:YLF laser by Lincoln *et al.*[135] points the way to a simpler oscillator, while the demonstration of beam shaping techniques for high power diode bar lasers [114], shows a direction for much higher average powers from Nd^{3+} based lasers. This latter, combined with KLM oscillators could provide sufficient oscillator output levels for efficient single pass harmonic generation, thus avoiding the complexity of resonant doubling. In fact such an arrangement would then completely remove the need for cavity stabilisation to interferometric precision, and one would be left only with the much more relaxed requirement of OPO cavity stabilisation as we have described here.

Acknowledgements.

This research has been supported by the UK Engineering and Physical Sciences Research Council. S.D. Butterworth thanks EPSRC and Lumonics Ltd., Rugby for support in the form of a CASE research studentship. S. Girard would like to thank the European Community for support in the form of a Human Capital and Mobility Fellowship grant. We would also like to thank Fujian Castech, and Photox for suppling the LBO crystals used in the n_2 measurements and finally E. W. Van Stryland and A. Dogariu from CREOL, University of Central Florida, for performing the z-scan measurements on the LBO samples.

Figure captions:

Figure 1: Schematic of longitudinally diode-pumped Nd:YLF amplifier.

Figure 2: Output power versus input power of the Nd:YLF amplifier.

Figure 3: Second harmonic output power at 523.5nm versus input coupler reflectivity. Data points-circles; normalised data-solid curve; theoretical output-dotted curve.

Figure 4: Interferometric autocorrelation trace of frequency doubled pulses.

Figure 5: Cavity configurations for the OPO: with and without intracavity dispersion compensation.

Figure 6: Output power of the OPO across the tuning range with three different mirror sets: (a) signal and (b) idler. Top traces are with Nd:YLF amplifier and fully optimised resonant frequency doubler. Bottom traces are without the amplifier.

Figure 7: Wavelength versus temperature tuning for the OPO. Solid line using Sellmeier equations of Lin *et al.* [23]. Dotted line using Sellmeier equations of Kato [24].

Figure 8: Intensity autocorrelation traces (a) and corresponding power spectrum (b) at different levels of circulating signal power without intracavity GVD compensation. Interferometric autocorrelation trace (c). The traces in figures 8(a,b) have been offset for clarity.

Figure 9: Variation of the average signal output power with relative cavity-length detuning.

Figure 10: Intensity autocorrelation trace (a) and corresponding power spectrum (b) with intracavity prism pair. Interferometric autocorrelation (c) at maximum circulating power with 4mm of SF10 glass.

References:

1. P. E. Powers, R. J. Ellingson, W. S. Pelouch and C. L. Tang, "Recent advances of the Ti:sapphire-pumped high-repetition-rate femtosecond optical parametric oscillator.", J. Opt. Soc. Am. B., **10**, p.2162-2167 (1993), See also associated literature in the same special issue on synchronously pumped optical parametric oscillators.

2. J. Goodberlet, J. Jacobson, J. G. Fujimoto, P. A. Schulz and T. Y. Fan, "Self-starting additive-pulse-mode-locked diode-pumped Nd:YAG laser", Optics Lett., **15**, p.504-506 (1990).

3. M. J. McCarthy, G. T. Maker and D. C. Hanna, "Efficient frequency doubling of a self-starting additive-pulse mode-locked diode pumped Nd:YAG laser", Optics Commun. **82**, p.327-332, (1991).

4. A. Robertson, and A. I. Ferguson, "Synchronously pumped all-solid-state lithium triborate optical parametric oscillator in a ring configuration", Optics Lett., **19**, p.117-119, (1994).

5. M. J. McCarthy, S. D. Butterworth and D. C. Hanna, "High-power widely-tunable picosecond pulses from an all-solid-state synchronously-pumped optical parametric oscillator", Optics Commun., **102**, p.297-303, (1993).

6. S. D. Butterworth, M. J. McCarthy and D. C. Hanna, "Efficient operation of an all-solid-state synchronously-pumped lithium triborate optical parametric oscillator", OSA proceedings on Advanced Solid State Lasers, Vol. 20, eds. T. Y. Fan and B. H. T. Chai, p.421-424, (1994).

7. E. S. Wachman, D. C. Edelstein and C. L. Tang, "Continuous wave mode-locked and dispersion compensated femtosecond optical parametric oscillator", Optics Lett. **15**, p.136-138, (1990).

8. J. M. Dudley, D. T. Reid, M. Ebrahimzadeh and W. Sibbett, "Characteristics of a noncritically phasematched Ti:sapphire pumped femtosecond optical parametric oscillator", Optics Commun., **104**, p.419-430, (1994).

9. M. J. McCarthy and D. C. Hanna, "Continuous-wave mode-locked singly resonant optical parametric oscillator synchronously pumped by a laser-diode-pumped Nd:YLF laser", Optics. Lett., **17**, p.402-404 (1992).

10. M. J. McCarthy, "Investigation of an all solid state synchronously pumped optical parametric oscillator", PhD Thesis, Southampton University, 1992

11. G. P. A. Malcolm, P. F. Curley, A. I. Ferguson,"Additive-pulse mode locking of a diode-pumped Nd:YLF laser", Optics. Lett., **15**, p.1303-1305 (1990).

12. D. W. Hughes, A. A. Majdabadi, J. R. M. Barr and D. C. Hanna, "Sub-picosecond Pulse generation from a Laser-Diode-Pumped, Self-Starting Additive-Pulse Mode-Locked Nd:LMA", OSA Proceedings on Advanced Solid-State Lasers, Vol.15, p.233-237 (1993).

13 J. R. Ryan and R. Beach, "Optical absorption and stimulated emission of neodymium in yttrium lithium fluoride", J. Opt. Soc. Am. B, **9**, p.1883-1887 (1992).

14. W. A. Clarkson, A. B. Neilson and D. C. Hanna, "Diode laser bar beam shaping technique", Conference on Lasers and Electro-optics Europe, Technical Digest, Paper CFH6, p.410-411, (1994)

15. A. Ashkin, G. D. Boyd, J. M. Dziedzic, "Resonant optical second harmonic generation and mixing", IEEE J. Quantum Electron., **2**, p.109-124 (1966)

16. W. J. Koslovsky, C. D. Nabors and R. L. Byer, "Efficient second harmonic generation of a diode-laser-pumped CW Nd:YAG laser using monolithic MgO:$LiNbO_3$ external resonant cavity", IEEE J. Quantum Electron, **24**, p.913-919, (1988)

17. M. A. Persaud, J. M. Tolchard, A. I. Ferguson, "Efficient generation of picosecond pulses at 243nm", IEEE J. Quantum Electron., **26**, p.1253-1258 (1990).

18. A. Yariv, "Quantum Electronics", third edition, p.398-400, (New York; Wiley, 1989).

19. R. W. P. Drever, J. L. Hall, F. V. Kowalski, J. Hough, G. M. Ford, A. J. Munley and H. Ward, "Laser phase and frequency stabilisation using an optical resonator", Appl. Phys. B31, p.97-105 (1983).

20. G. D. Boyd and D. A. Kleinman, "Parametric interaction of focused Gaussian light beams", J. Appl. Phys., **39**, p.3597-3639 (1966).

21. M. J. McCarthy and D. C.Hanna, "All-solid-state synchronously pumped optical parametric oscillator", J.Opt. Soc. Am. B., **10**, p.2180-2190, (1993)

22. S. Guha, F. Wu, J. Falk, "The effects of focussing on parametric oscillation", IEEE J. Quantum. Electron., **QE-18**, p.907-912, (1982).

23. S. Lin, B. Wu, F. Xie and C. Chen, "Phase-matching retracing behaviour: new features in LiB_3O_5", Appl. Phys. Lett., **59**, p.1541-1543 (1991).

24. K. Kato "Temperature-tuned 90° phase-matching properties of LiB_3O_5", IEEE J. Quantum Electron., **30**, p.2950-2952, (1994)

25. J. C. Diels, J. J. Fontaine, I. C. McMichael and F. Simoni, "Control and measurement of ultrashort pulse shapes (in amplitude and phase) with femtosecond accuracy", Applied Optics, **24**, p.1270-1282 (1985).

26. G. I. Stegeman, M. Sheik-Bahae, E. W. Van Stryland and G. Assando, "Large nonlinear phase shifts in second-order nonlinear-optical processes", Optics. Lett., **18**, p.13-15 (1993).

27. Q. Fu, G. Mak and H. M. Van Driel, "High-power, 62-fs infrared optical parametric oscillator synchronously pumped by a 76MHz Ti:sapphire laser", Optics Lett. **17**, p.1006-1008, (1992).

28. W. S. Pelouch, P. E. Powers and C. L. Tang, "Ti:sapphire-pumped, high-repetition-rate femtosecond optical parametric oscillator", Optics. Lett., **17**, p.1070-1072, (1992).

29. E. W. Van Stryland and A. Dogariu, Centre for Research and Education in Optics and Lasers, 12424 Research Parkway, Suite 400, Orlando, Florida 32826 (private communication, October 1994)

30. J. Chesnoy and L. Fini, "Stabilization of a femtosecond dye laser synchronously pumped by a frequency-doubled mode-locked YAG laser", Optics. Lett., **11**, p.635-637 (1986).

31. S. D. Butterworth, S. Girard and D. C. Hanna, "A simple technique for active cavity-length stabilisation for a synchronously pumped optical parametric oscillator", submitted to Optics Communications.

32. R. L. Fork, C. H. Brito Cruz, P. C. Becker and C. V. Shank, "Compression of optical pulses to six femtoseconds by using cubic phase compensation", Optics Lett., **12**, p.483-485 (1987).

33.Z. Zhang and T. Yagi, "Observation of group delay dispersion as a function of the pulse width in a mode-locked Ti:sapphire laser", Appl. Phys. Lett., **63**, p.2993-2995 (1993).

34. Optical Glass, Schott Catalogue.

35. J. R. Lincoln, I. M. Botheroyd and A. I. Ferguson, "Self mode-locking of Nd doped gain media in a simple X-fold cavity", Conference on Lasers and Electro-optics Europe, Postdeadline paper CPD1.7, p.13-14 (1994)

Fig 1.

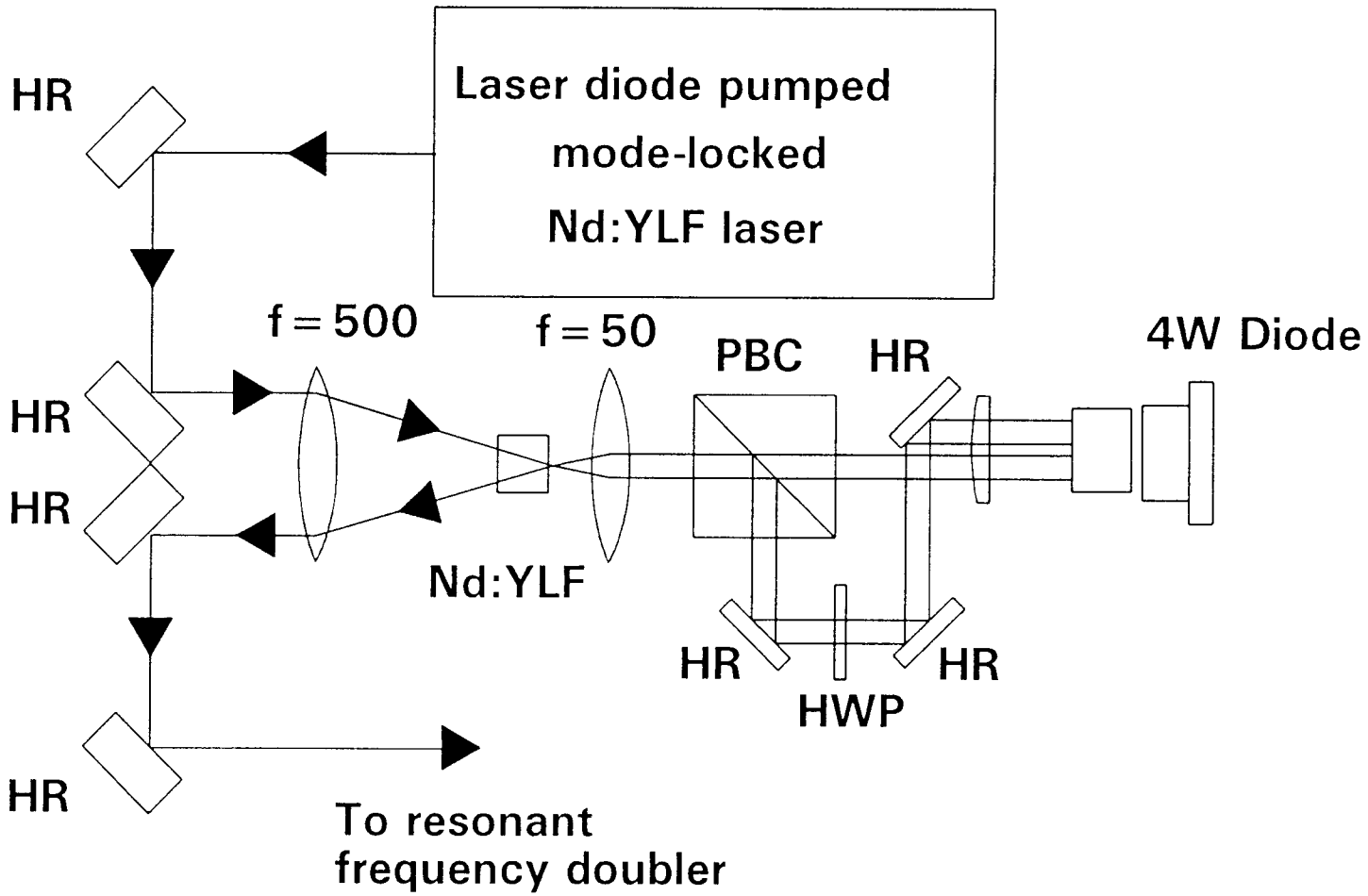
Laser diode pumped
mode-locked
Nd:YLF laser
HR
HR
HR
HR
f = 500
f = 50
PBC
HR
4W Diode
Nd:YLF
HR
HR
HWP
To resonant
frequency doubler

Fig 2

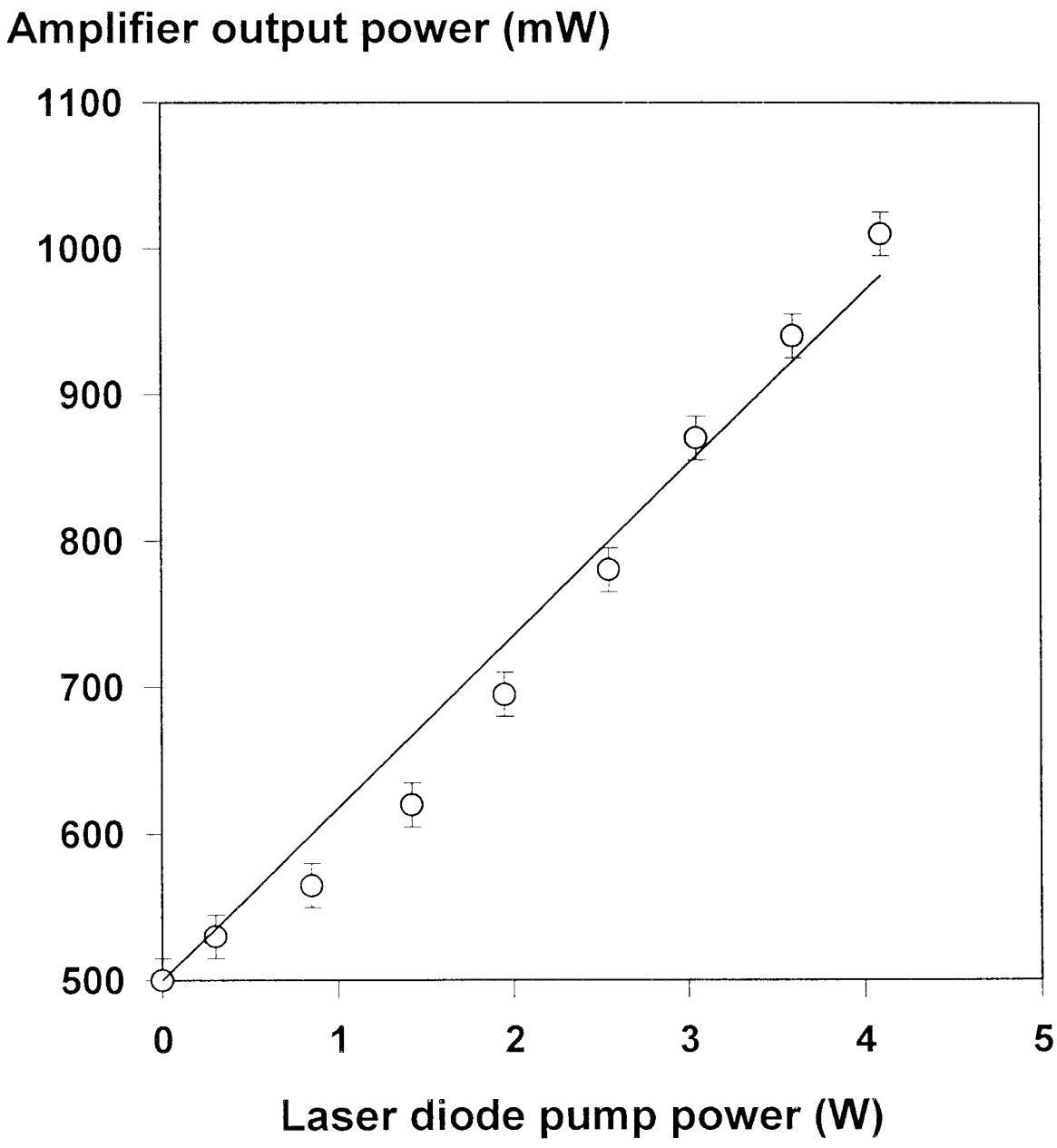
Amplifier output power (mW)
1100
1000
900
800
700
600
500
0
1
2
3
4
5
Laser diode pump power (W)

Fig 3

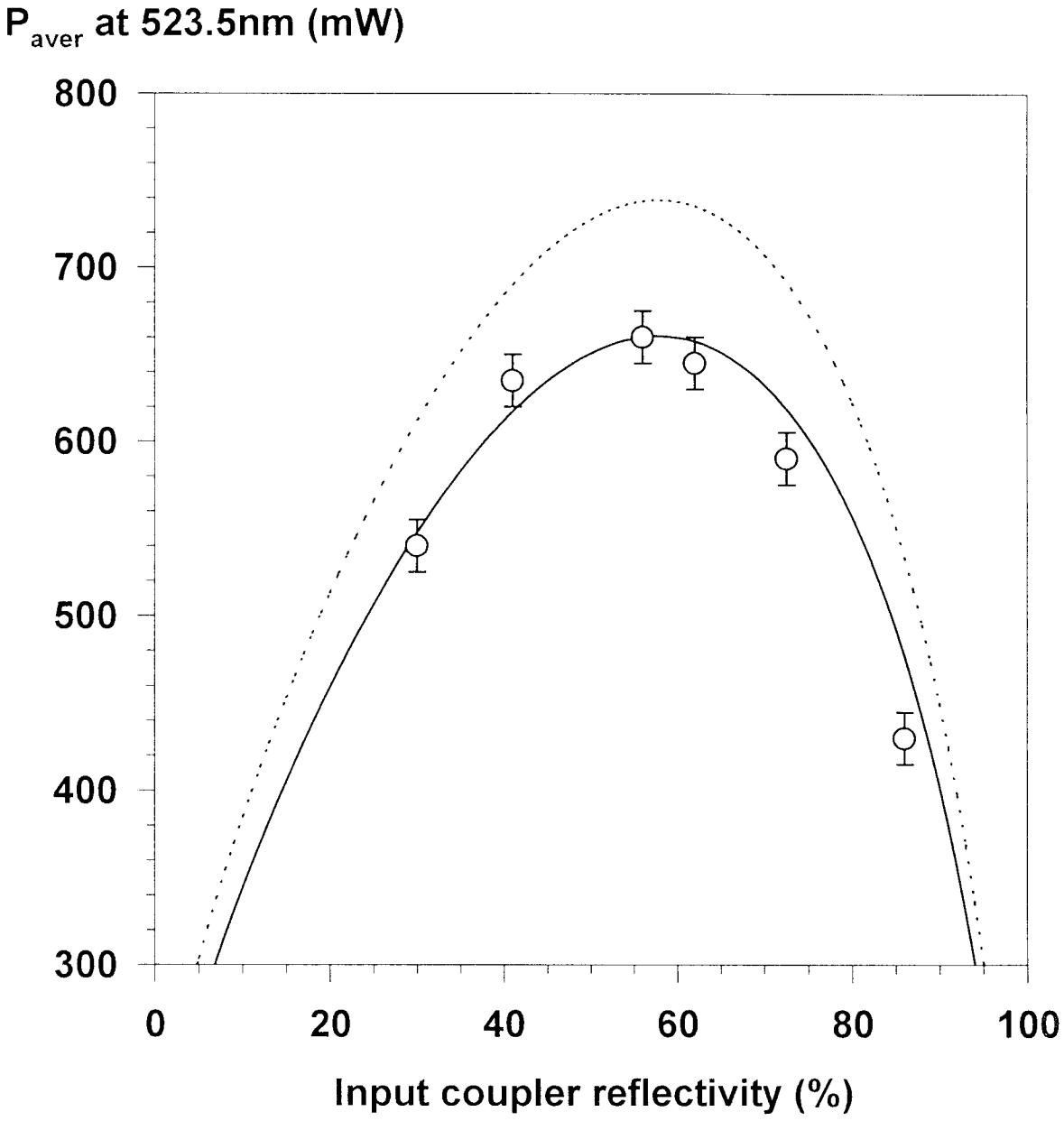
P aver at 523.5nm (mW)
800
700
600
500
400
300
0
20
40
60
80
100
Input coupler reflectivity (%)

Fig 4

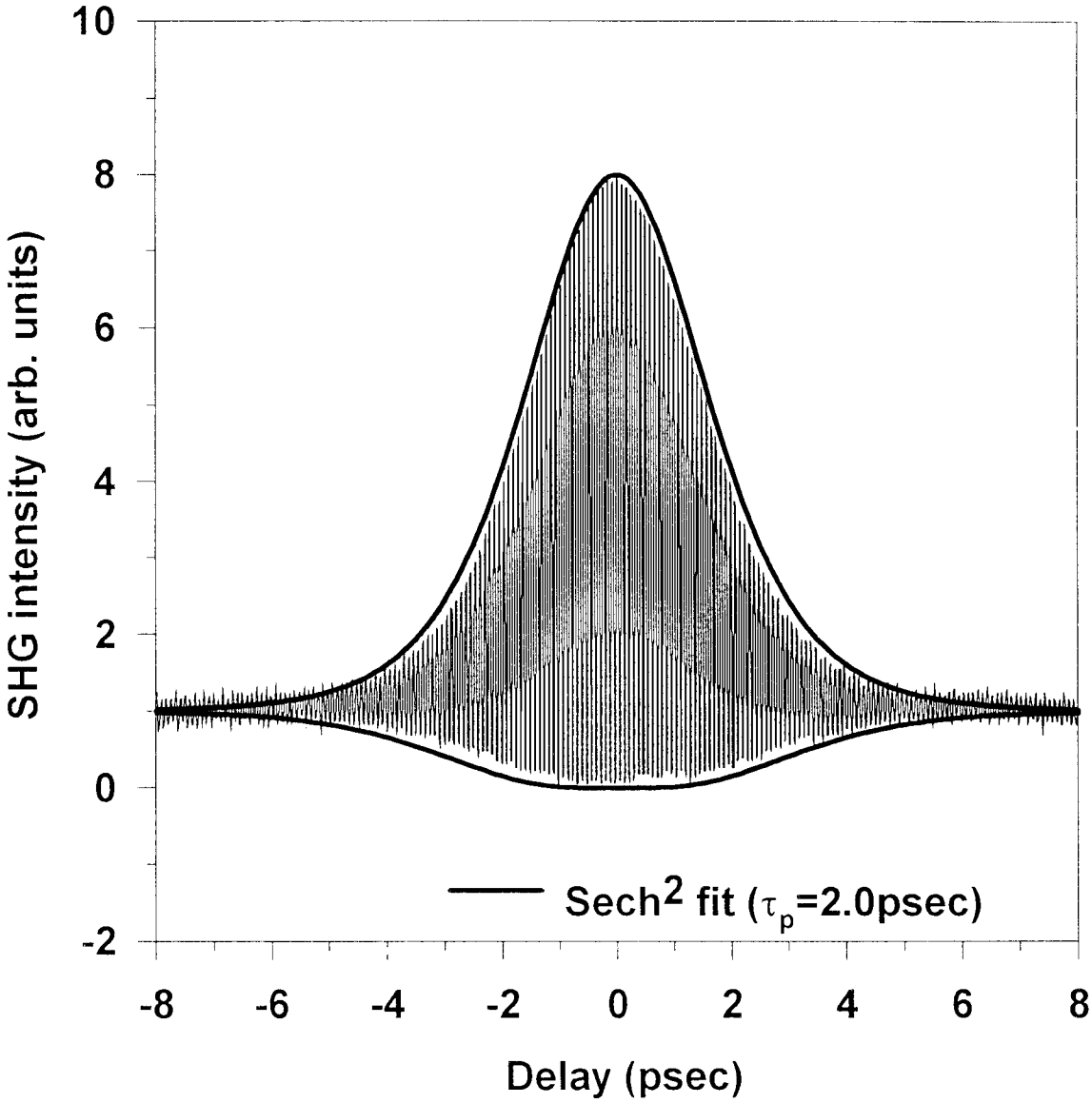
10
8
6
4
2
0
-2
SHG intensity (arb. units)
-8
-6
-4
-2
0
2
4
6
8
Delay (psec)
Sech2 fit (τp=2.0psec)

Fig 5

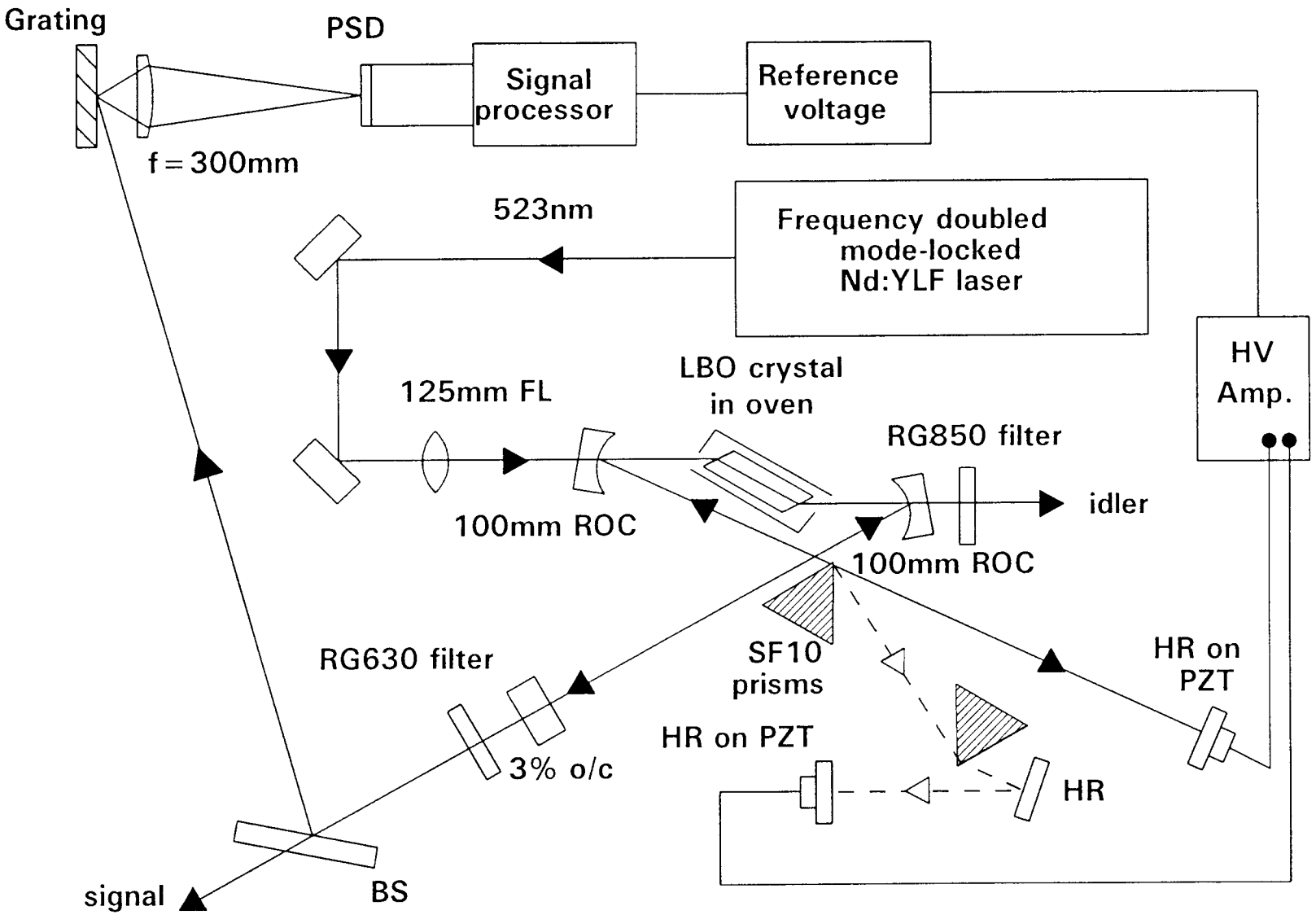
Grating
PSD
Signal processor
Reference voltage
f = 300mm
523nm
Frequency doubled mode-locked Nd:YLF laser
HV Amp.
125mm FL
LBO crystal in oven
RG850 filter
idler
100mm ROC
100mm ROC
SF10 prisms
RG630 filter
HR on PZT
HR on PZT
3% o/c
HR
signal
BS

Fig. 1(a)

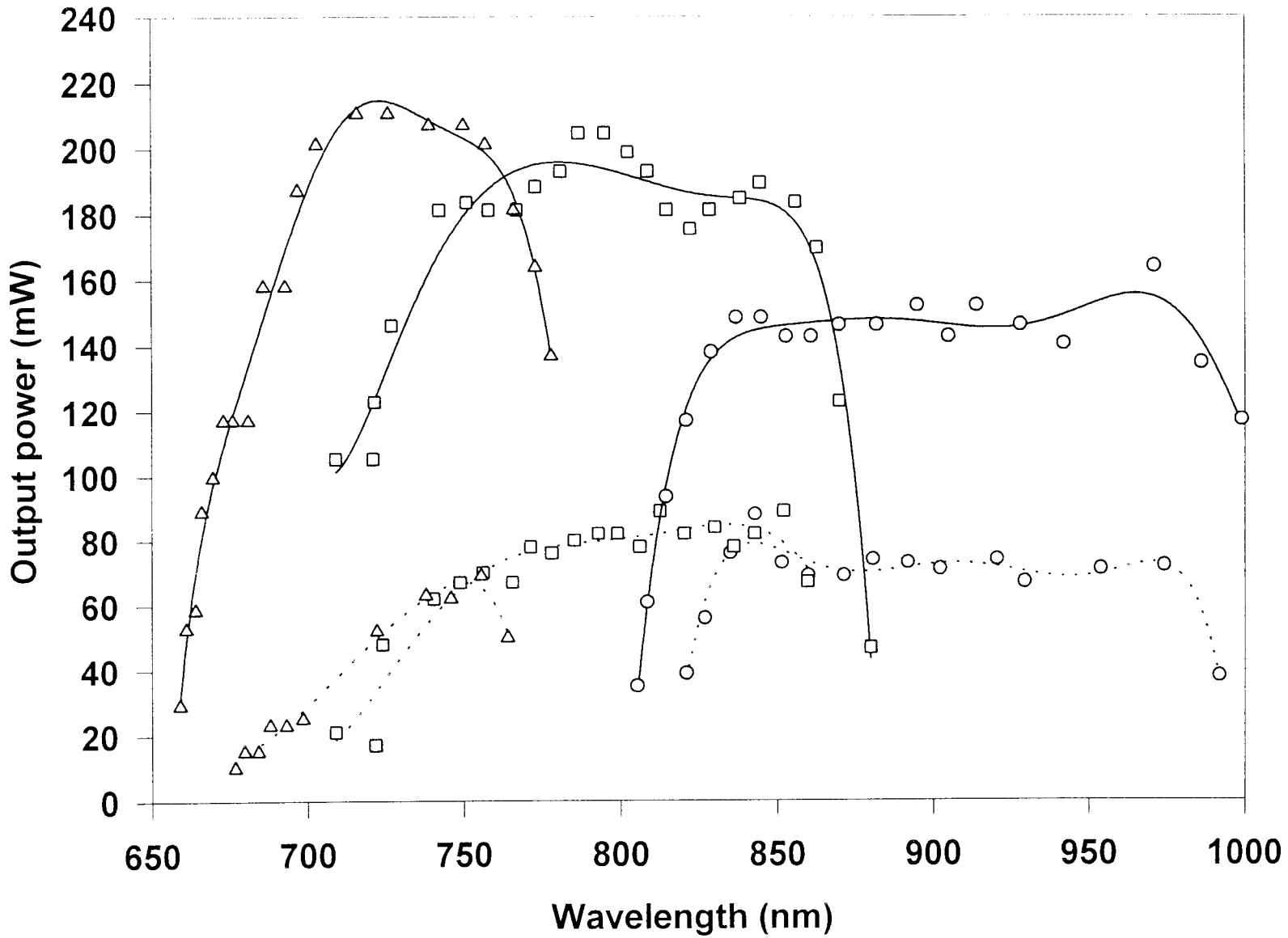
Output power (mW)
240
220
200
180
160
140
120
100
80
60
40
20
0
650
700
750
800
850
900
950
1000
Wavelength (nm)

Fig 6(b)

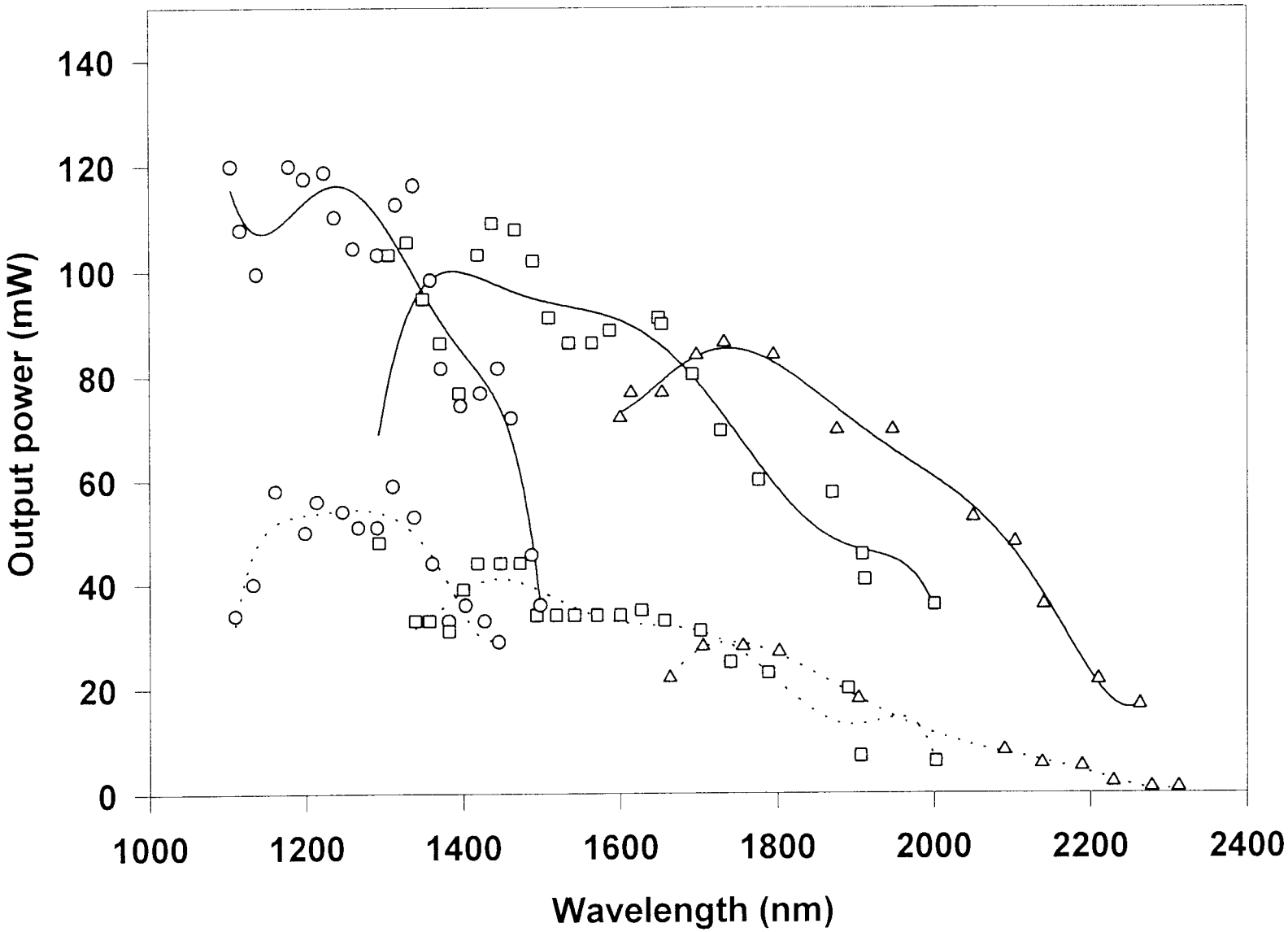
Output power (mW)
140
120
100
80
60
40
20
0
1000
1200
1400
1600
1800
2000
2200
2400
Wavelength (nm)

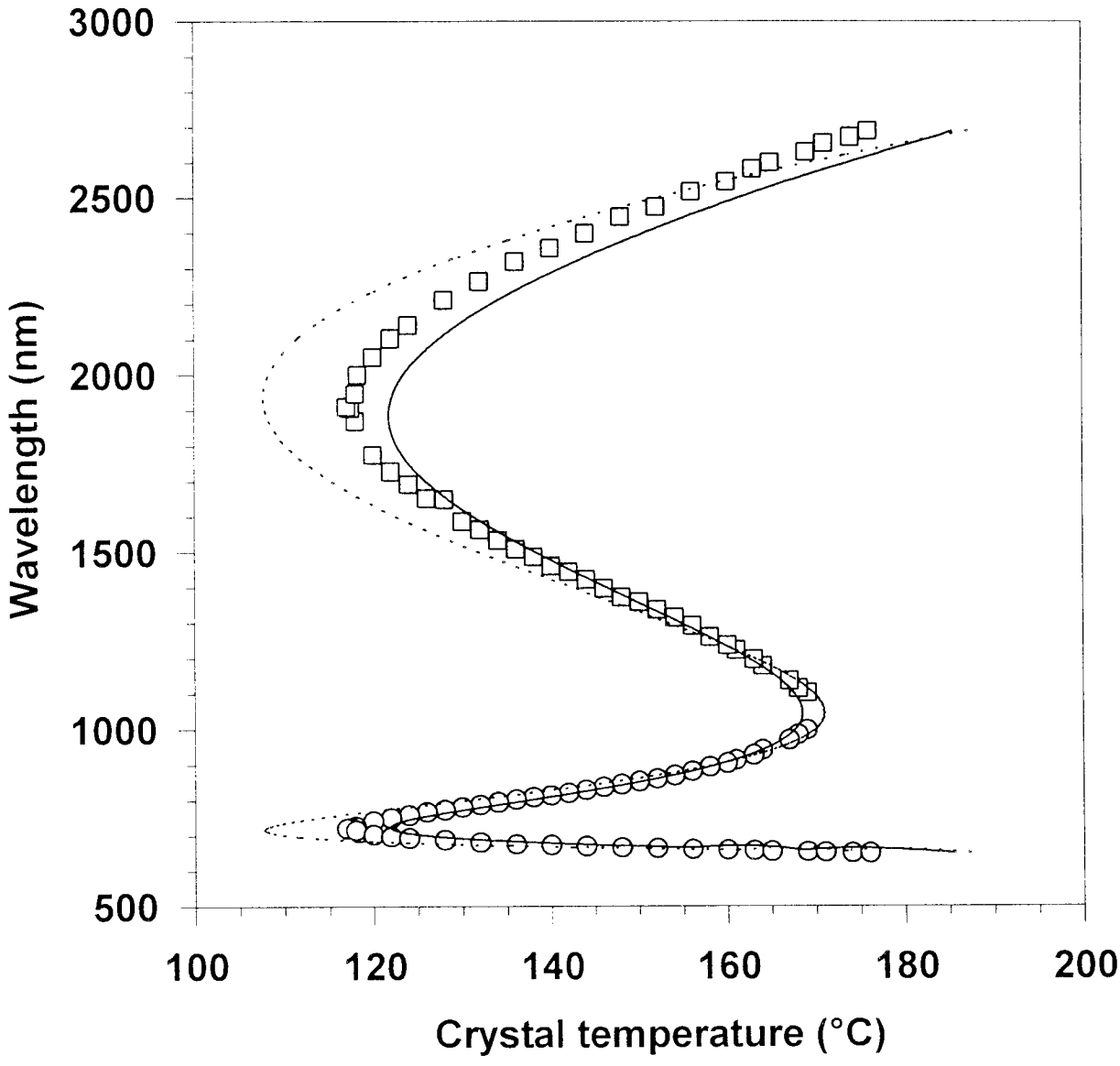
3000
2500
2000
1500
1000
500
Wavelength (nm)
100
120
140
160
180
200
Crystal temperature (°C)

Fig 8(c)

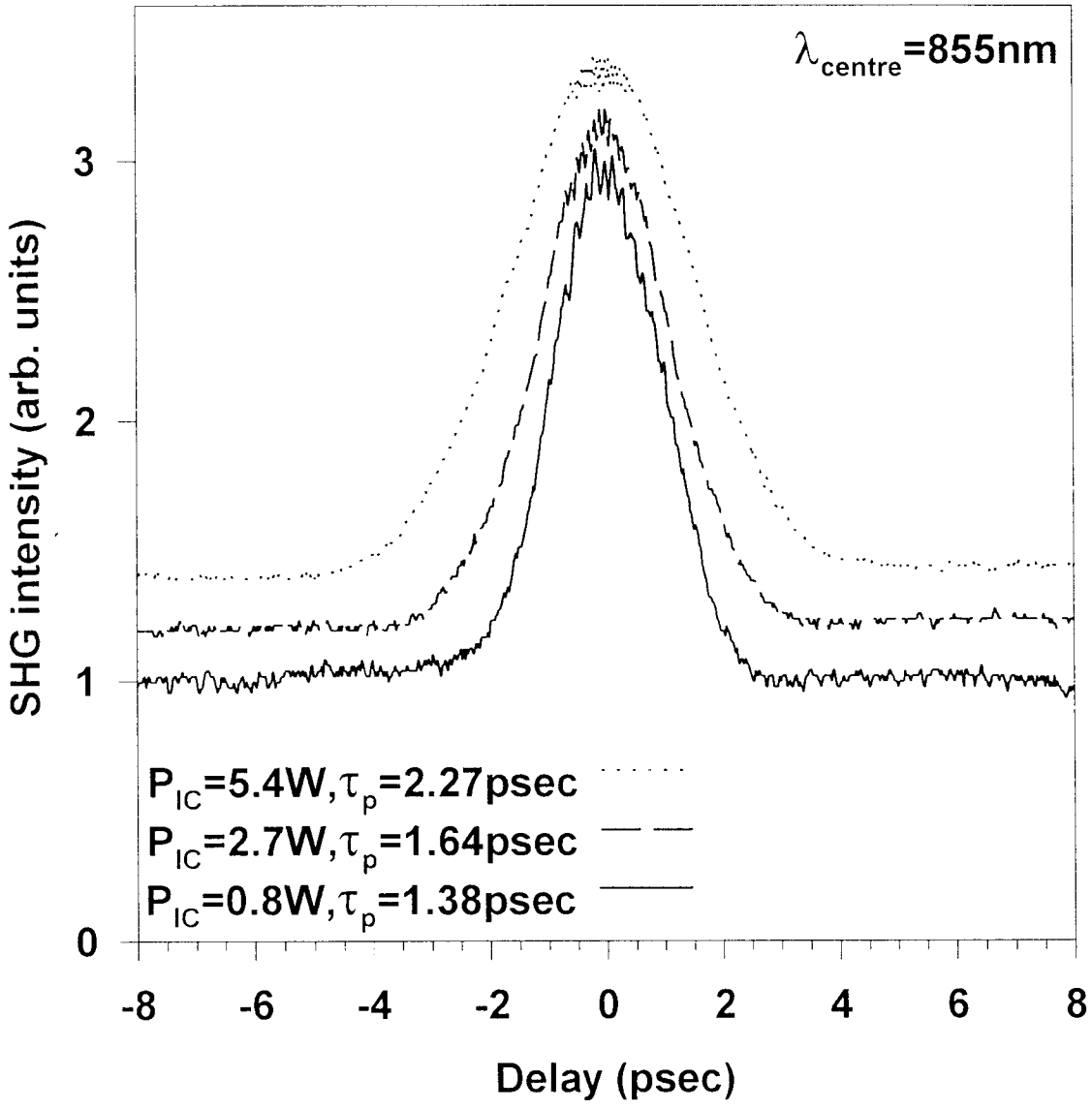
λcentre=855nm
SHG intensity (arb. units)
0
1
2
3
-8
-6
-4
-2
0
2
4
6
8
Delay (psec)
PIC=5.4W,τp=2.27psec
PIC=2.7W,τp=1.64psec
PIC=0.8W,τp=1.38psec

Fig 9(b)

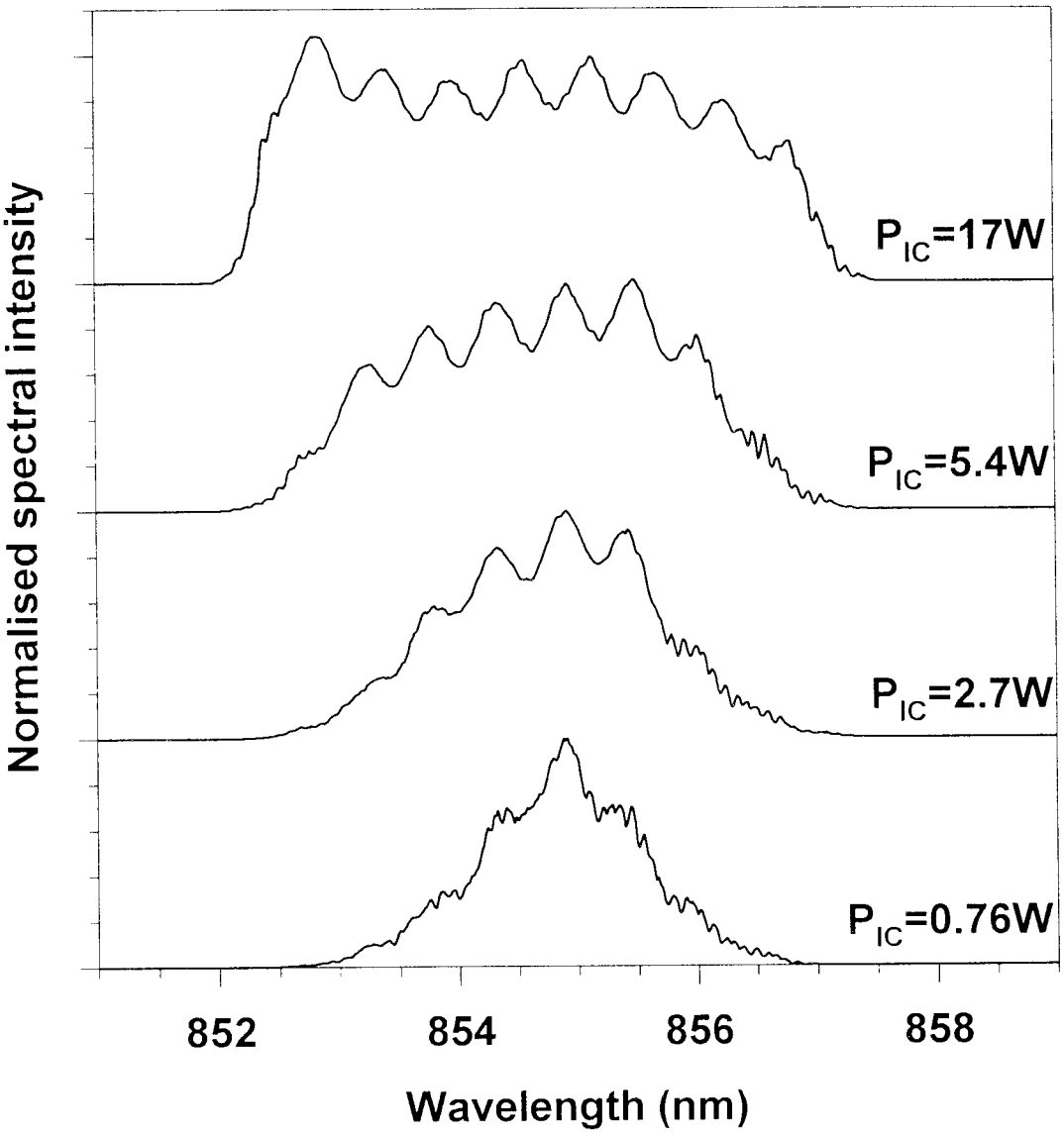
Normalised spectral intensity
P_IC=17W
P_IC=5.4W
P_IC=2.7W
P_IC=0.76W
852
854
856
858
Wavelength (nm)

Fig 9(c)

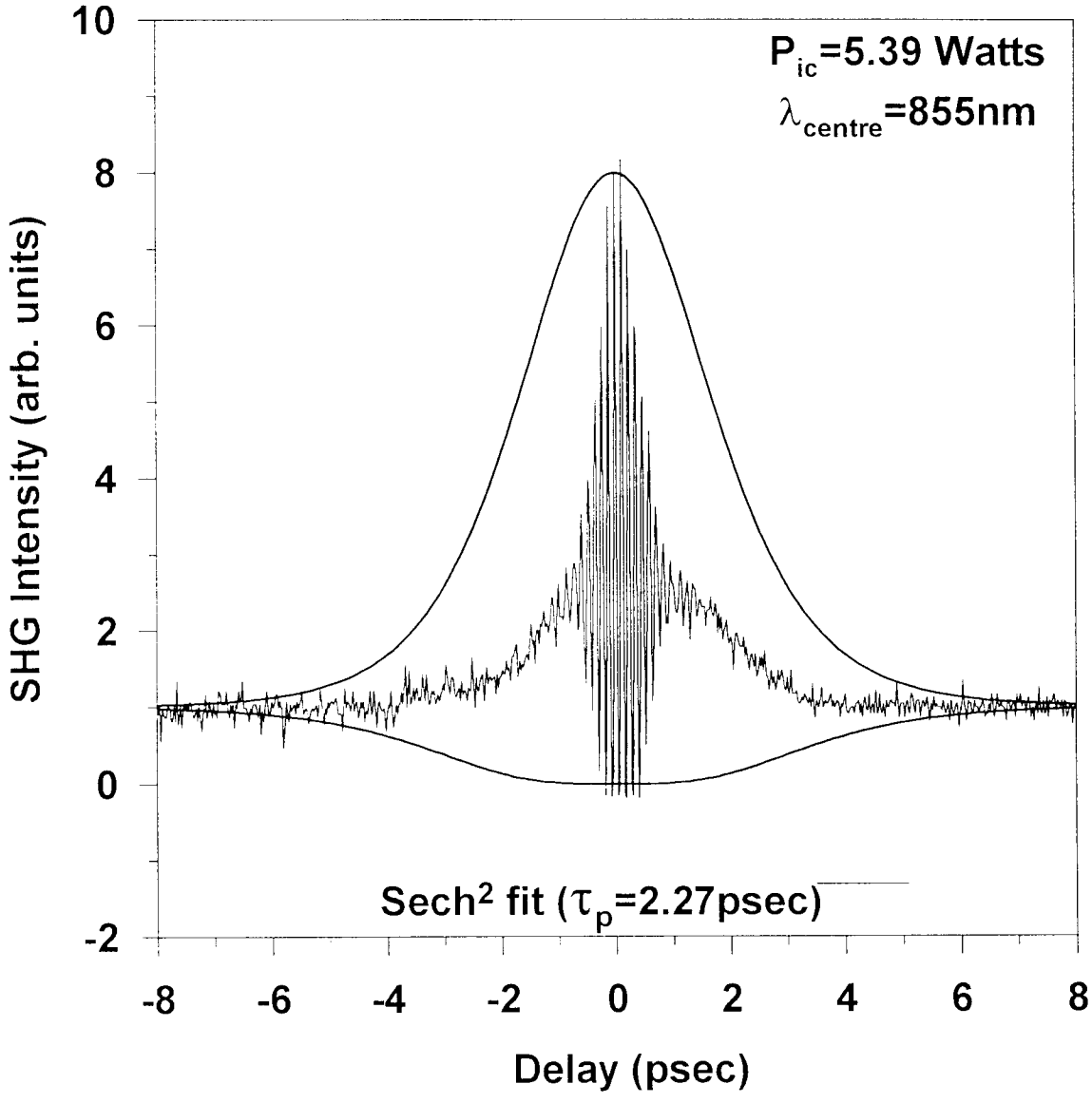
P_{ic}=5.39 Watts
λ_{centre}=855nm
Sech^2 fit (τ_p=2.27psec)
SHG Intensity (arb. units)
Delay (psec)
10
8
6
4
2
0
-2
-8
-6
-4
-2
0
2
4
6
8

Fig. 9

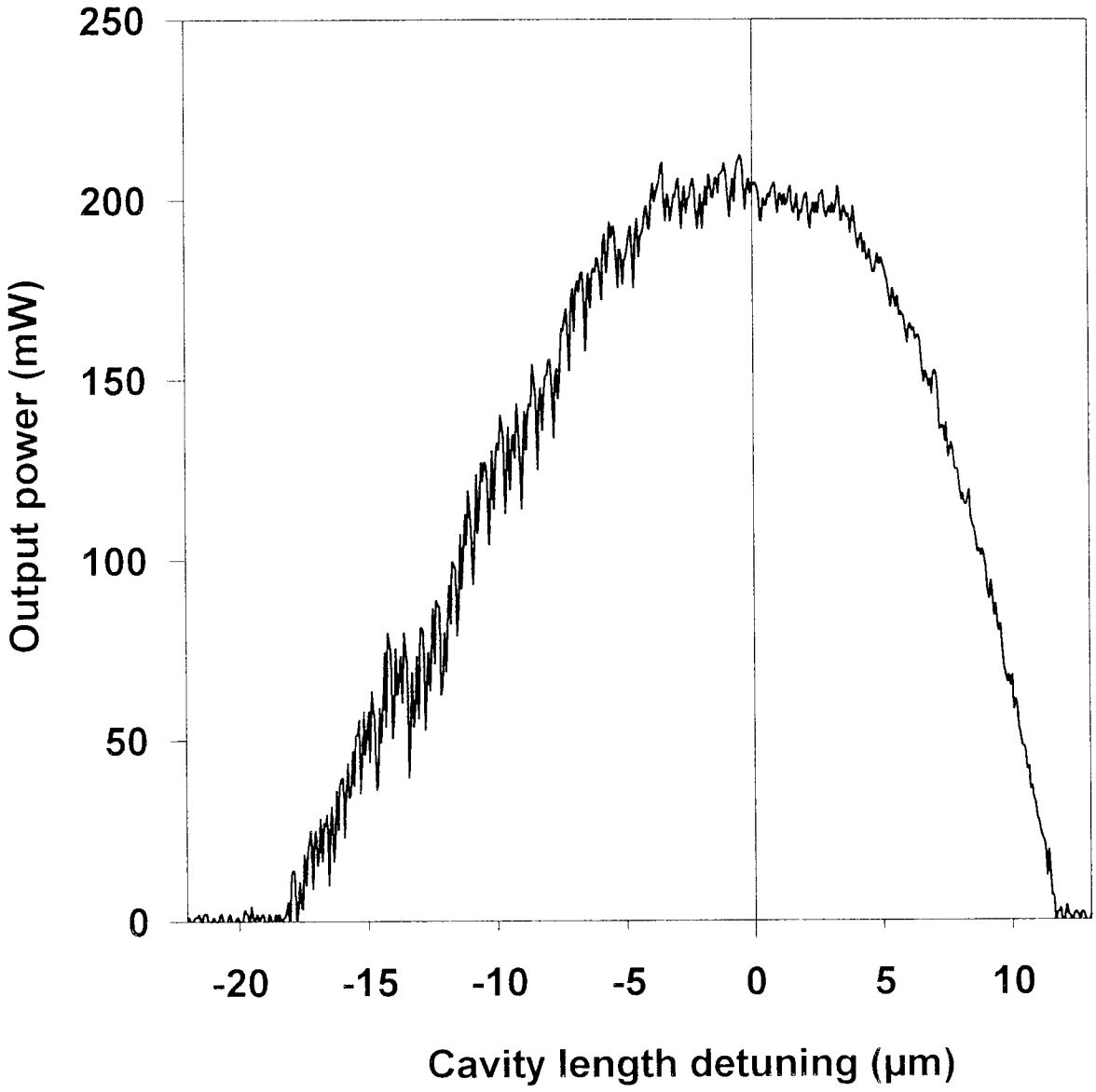
250
200
150
100
50
0
Output power (mW)
-20
-15
-10
-5
0
5
10
Cavity length detuning (μm)

fig 10(a)

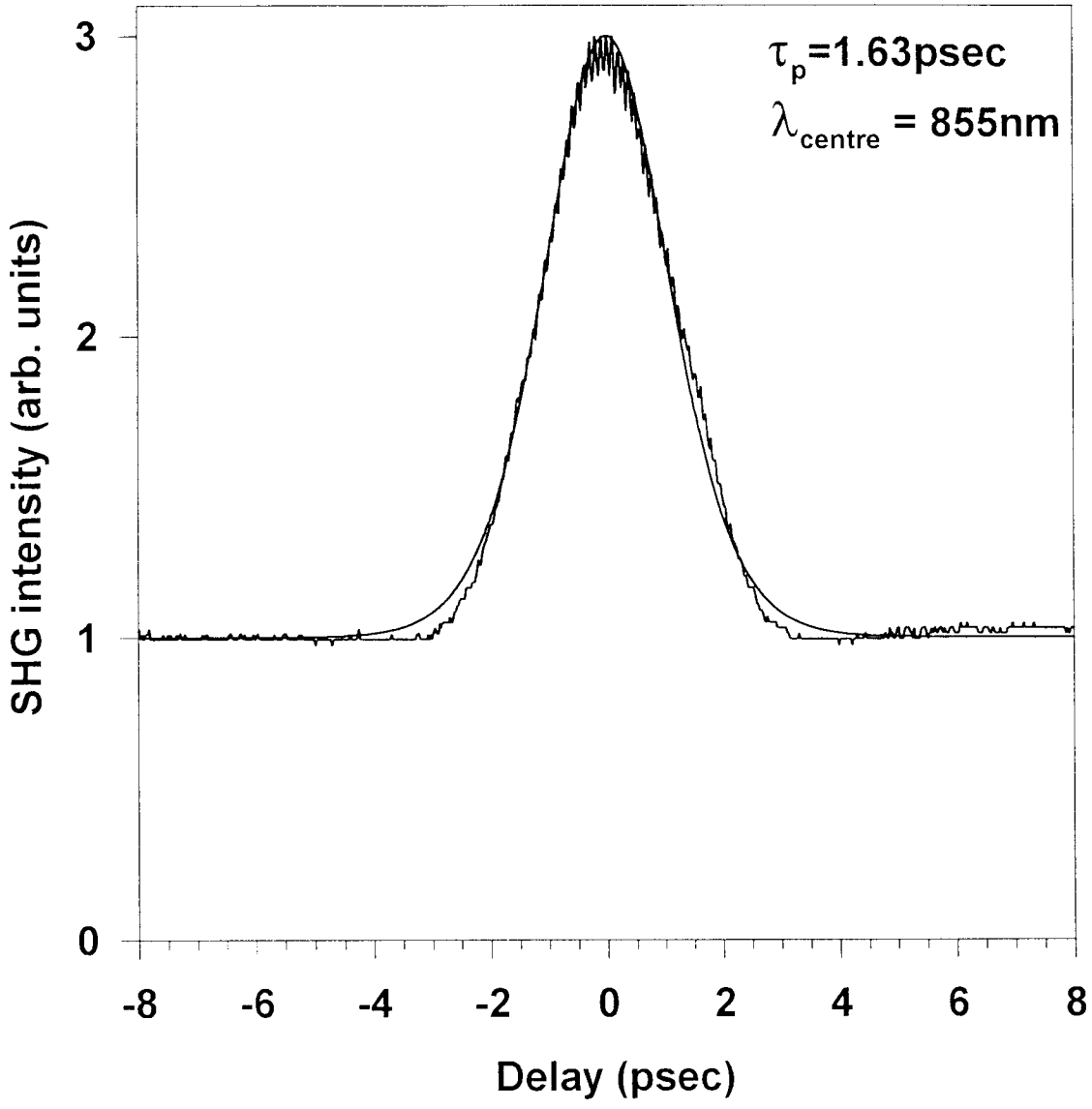
τ_p=1.63psec
λ_{centre} = 855nm
SHG intensity (arb. units)
Delay (psec)
0
1
2
3
-8
-6
-4
-2
0
2
4
6
8

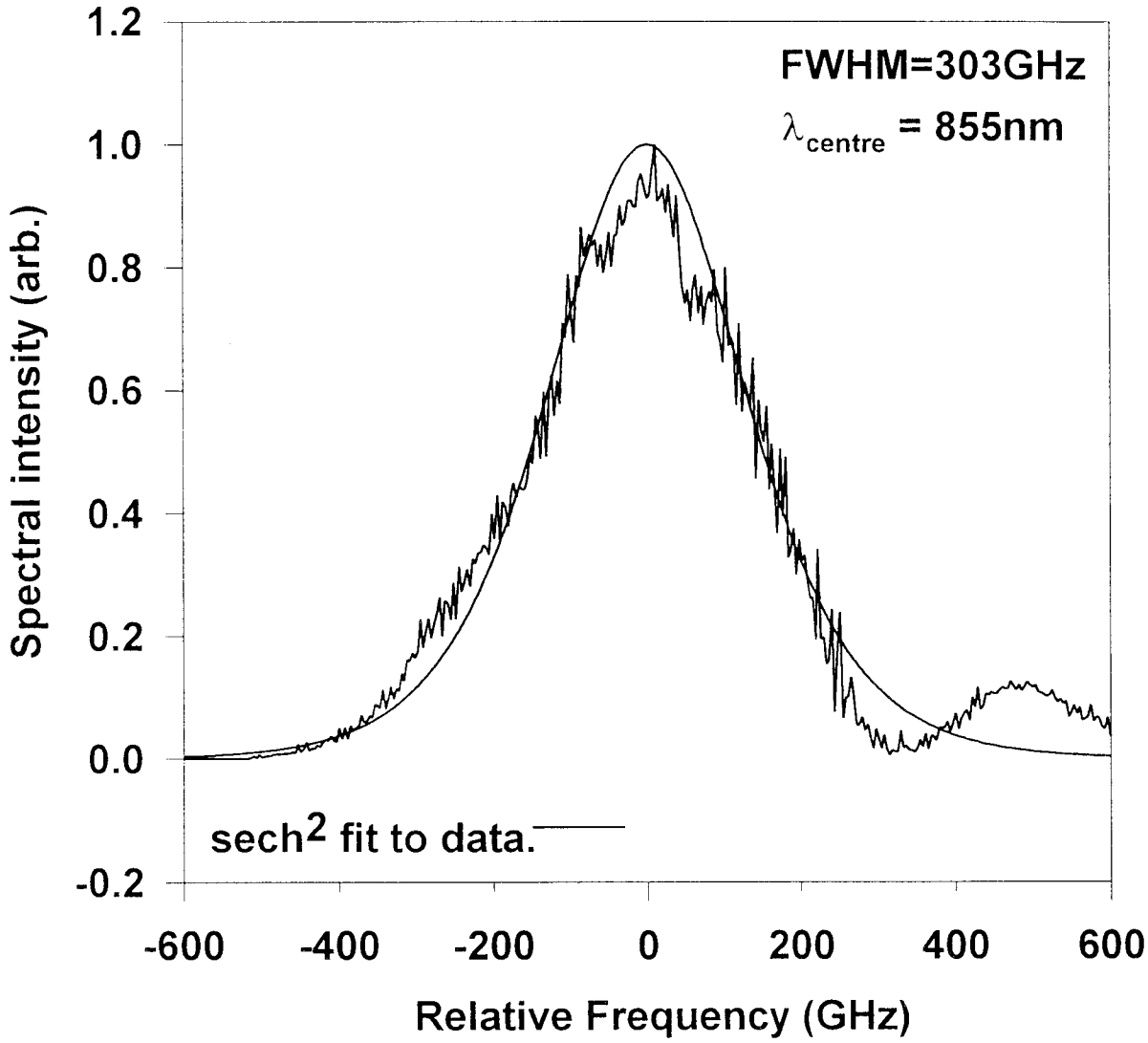
FWHM=303GHz
λcentre = 855nm
sech2 fit to data.
Spectral intensity (arb.)
Relative Frequency (GHz)
1.2
1.0
0.8
0.6
0.4
0.2
0.0
-0.2
-600
-400
-200
0
200
400
600

Fig 10(c)

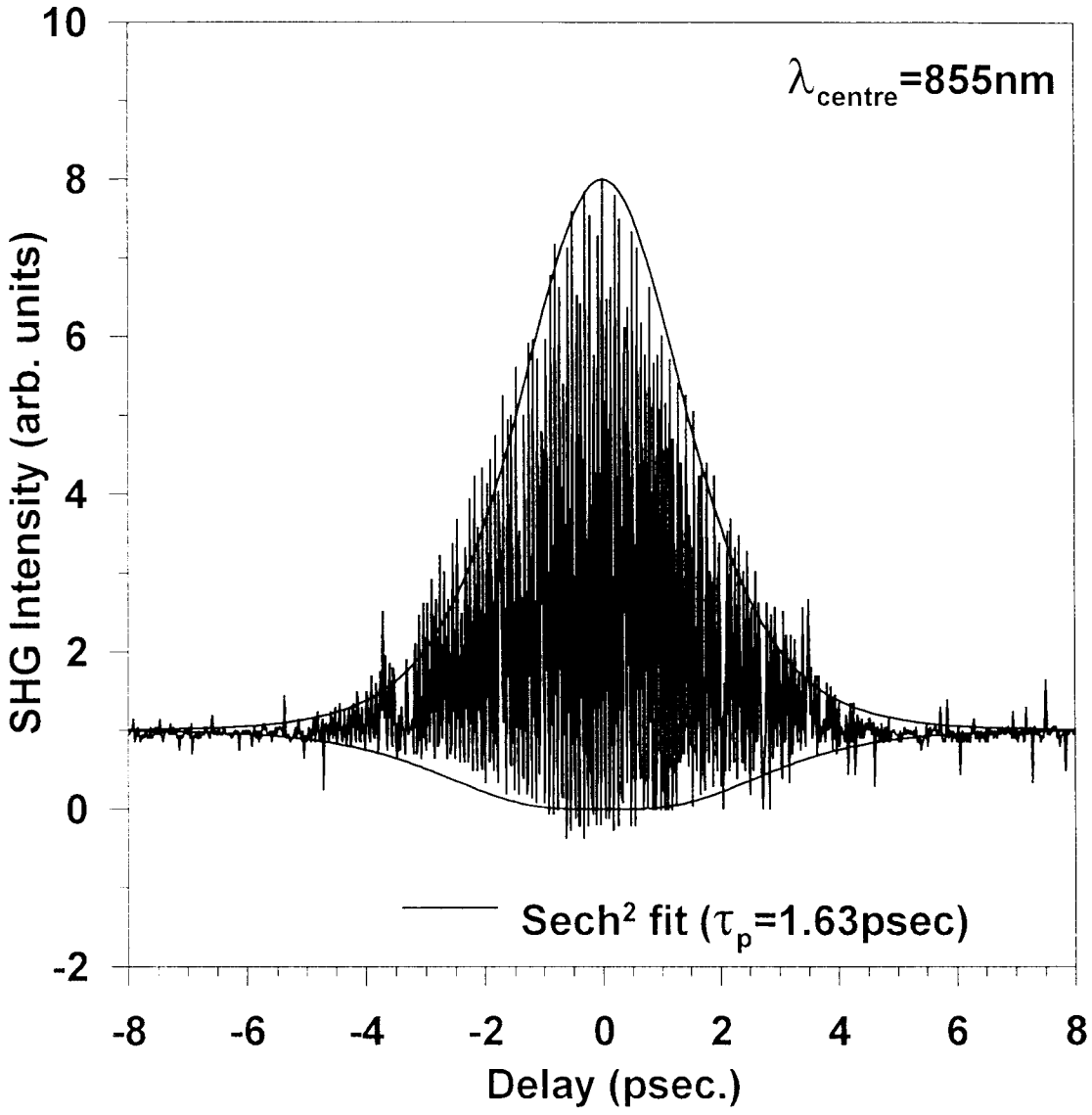
10
8
6
4
2
0
-2
SHG Intensity (arb. units)
λcentre=855nm
Sech² fit (τp=1.63psec)
-8
-6
-4
-2
0
2
4
6
8
Delay (psec.)